

MODELLING OF BLUE WAVELENGTH PRASEODYMIUM WAVEGUIDE LASERS

M. MALINOWSKI^a, A. MOSSAKOWSKA-WYSZYŃSKA^a, R. PIRAMIDOWICZ^a,
P. SZCZEPAŃSKI^a, A. TYSZKA-ZAWADZKA^a, Z. FRUKACZ^b AND I. PRACKA^b

^aInstitute of Microelectronics and Optoelectronics P.W.
Koszykowa 75, 00-662 Warsaw, Poland

^bInstitute of Electronic Materials Technology, Wólczyńska 133, 01-919 Warsaw, Poland

(Received October 13, 1999)

Emission and absorption spectra, lifetimes, and branching ratios in the blue spectral region have been experimentally determined for numerous oxide, fluoride and phosphate materials doped with Pr³⁺ ions. The emission cross-sections have been evaluated using the principle of reciprocity. A theoretical model allowing a prediction of the blue lasing characteristics of the praseodymium activated waveguide structures has been developed and employed to the investigated materials.

PACS numbers: 42.70.Hj, 78.20.-e, 78.55.Hx

1. Introduction

Recently, there is an interest in developing compact, short wavelength, all solid-state laser sources for display [1], optical data storage [2, 3], laser printing, under water communication [4], material processing and medical applications. Perspectively, high bandgap A₂B₆ semiconductors offer interesting prospects for visible diode lasers [5] but till now gallium arsenide (GaAs) remains the best developed infra-red diode-laser material.

The need for all compact solid-state devices makes the diode-pumped solid-state lasers the most promising approach. Diode laser-pumped solid-state lasers have the advantage of narrower linewidth, higher peak powers, and higher brightness compared to the direct use of diodes. Low cost, high power, and versatility have ensured that variation of GaAs lasers emitting between 750 and 900 nm are used as optical pumps. This, however, limits the number of possible laser transitions under diode laser pumping by the number of active elements with absorption at diode laser output. Thus, rare earth (RE) ions limited to Nd, Pr, Dy, Er, Yb, and Tm could be lased at IR wavelengths [6].

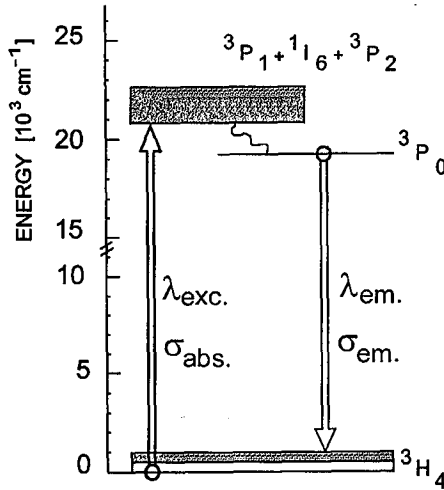


Fig. 1. Energy level diagram for Pr^{3+} ion showing excitation and blue emission transitions.

Short wavelength operation of diode laser pumped solid state laser systems could be produced by using nonlinear techniques. Thus, harmonic generation in nonlinear crystals [7] and frequency upconversion lasers [8, 9] are two promising techniques.

Trivalent praseodymium (Pr^{3+}) ion activated materials can lase in the visible range on the transitions originating from the excited 3P_0 state and terminating at different lower levels [9]. Transition terminating at the ground state, ${}^3P_0 \rightarrow {}^3H_4$, is in the blue part of the spectrum and is effectively a three-level system, see Fig. 1. Several factors influence the performance of this laser scheme. The 3H_4 ground state is split into several Stark levels extending over about 600 cm^{-1} . Since the lowest Stark component at 0 cm^{-1} is substantially thermally populated and because of signal reabsorption, in most cases, the blue laser action terminates at one of the higher Stark levels in the ground multiplet. Thus, the ground state splitting, especially the position of the second Stark level, is an important factor and should be considered in the evaluation of the blue laser performances. Also, the branching ratio β for the ${}^3P_0 \rightarrow {}^3H_4$ transition has a significant impact on the threshold and efficiency of a laser. Another important property, that must be known in order to describe the characteristics of a luminescence device, is the emission cross-section σ .

Praseodymium ion has been demonstrated to lase in the 480–520 nm, blue-green region in various fluoride and oxide crystals, such as $\text{LiYF}_4:\text{Pr}^{3+}$ (YLF: Pr^{3+}) [10, 11], $\text{GdLiF}_4:\text{Pr}^{3+}$ [12], $\text{Y}_3\text{Al}_5\text{O}_{12}:\text{Pr}^{3+}$ (YAG: Pr^{3+}) [13, 14], $\text{YAlO}_3:\text{Pr}^{3+}$ (YAP: Pr^{3+}) [14] and $\text{Gd}_3\text{Ga}_5\text{O}_{12}:\text{Pr}^{3+}$ (GGG: Pr^{3+}) [14] under one photon pumping. Recently, Pr^{3+} activated fluoride fibers have been demonstrated to oscillate at short wavelengths under different upconversion excitation conditions [15–18]. While optical fibers and fiber amplifiers are used for telecommunication, planar integrated optics may be used for optical signal processing on a local scale. Also,

waveguide lasers offer several optogeometric advantages giving rise to low threshold, high slope efficiency, and stability. Liquid phase epitaxy [19, 20] and ion implantation [21, 22] have been proved to be a successful method of producing low loss rare earth doped planar lasers.

In this work, optical properties that impact the potential blue laser performance of praseodymium activated materials have been measured. In particular, we measured energy of 3P_0 emitting level, lifetime, branching ratio, and emission cross-section spectra for blue, ${}^3P_0 \rightarrow {}^3H_4$ transition of Pr^{3+} in YAG, YAP, GGG, YLF, ZBLAN glass, LiNbO_3 (LNB), $\text{SrLaGa}_3\text{O}_7$ (SLG), $\text{Be}_2\text{La}_2\text{O}_5$ (BLO), and $\text{KPrP}_5\text{O}_{14}$ (KPP). Based on these data and in the framework of extended earlier models [23–25] the performance of the Pr-based waveguide lasers has been evaluated under one-photon pumping. In particular threshold conditions, output power, slope efficiency, and modulation bandwidth have been investigated. The two-photon pumping laser structures will be discussed in the further paper.

2. Experimental results

Nine samples of different laser materials doped with Pr^{3+} ions were investigated. All of the reported here spectroscopic data were obtained at room temperature. Absorption spectra were measured with a Perkin-Elmer Lambda 9 spectrometer. In the cases of optically anisotropic crystals: YLF, YAP, BLO, and KPP, polarised absorption spectra were measured. Luminescence was excited by a cw Carl Zeiss ILA 120 argon laser or a pulsed 1 MW nitrogen laser pumped dye laser. The spectra were recorded with a GDM-1000 monochromator equipped with a RCA C31034-02 photomultiplier and followed by a PC controlled Stanford SR400 single photon counting system. Fluorescence lifetime measurements were performed with an Oxford MCS-II multichannel analyser.

The crystal structure, active ion concentration, and the measured here 3P_0 upper level energy $E({}^3P_0)$, emission lifetime τ_{fl} , position of the second Stark level in the ground state manifold $E({}^3H_4(2))$ and the branching ratio for the blue transition β are listed in Table I. Theoretical values of β listed in the last column of Table I have been taken from the literature or calculated by us using Judd-Ofelt theory [26, 27], references to these works are given in the same column. In LiNbO_3 , probably due to efficient nonradiative relaxation, the observed 3P_0 fluorescence decay is rapid and emission from the 3P_0 level is very weak and masked by a relatively strong 1D_2 emission, making the determination of the ${}^3P_0 \rightarrow {}^3H_4$ branching ratio impossible.

The emission cross-sections of the 480 nm band have been evaluated using the absorption cross-section and the McCumbers principle of reciprocity [38]. According to [38] for the resonant transition the σ_{em} — emission cross-section — could be expressed in terms of the σ_{ab} — absorption cross-section — multiplied by the ratio of the partition functions Z_l/Z_u

$$\sigma_{\text{em}}(\nu) = \sigma_{\text{ab}}(\nu) \frac{Z_l}{Z_u}, \quad (1)$$

where $Z_m = \sum_m g_m \exp(-E_m/kT)$, g_m is the degeneracy of the m level and E_m is the energy of level m , k is Boltzmann constant, T is the temperature, and ν is

TABLE I

Structural and measured spectroscopic parameters of the Pr^{3+} ion in the investigated materials (τ_{fl} — measured fluorescence lifetime, E — energy of the state, β — branching ratio for the ${}^3P_0 \rightarrow {}^3H_4$ transition; in the third column the site coordination number is given).

Host	Structure symmetry optical class		Pr ³⁺ conc. [10 ²⁰ cm ⁻³] at %	E (³ P ₀) [cm ⁻¹]	τ_{fl} (³ P ₀) [μs]	E (³ H ₄ (2)) [cm ⁻¹]	β (³ P ₀ → ³ H ₄) [%]	
							theory	exp.
Y ₃ Al ₅ O ₁₂ (YAG)	garnet cubic isotropic	8	1.385 1%	20534	12	19	71	63 [13, 28]
Gd ₃ Ga ₅ O ₁₂ (GGG)	garnet cubic isotropic	8	1.229 1%	20600	14	26	76	47 [29]
YAlO ₃ (YAP)	perovskite orthorombic biaxial	12	0.83 0.3%	20417	11	51	55	70 [30]
LiYF ₄ (YLF)	scheelite tetragonal uniaxial	8	1.39 1%	20866	38	81	71	38 [31, 32]
ZBLAN	glass	—	0.0685	20920	40		52	42 [33, 34]
LiNbO ₃ (LNB)	ilmenit trigonal uniaxial	8	1.6 1%	19890	0.45	275	69	[35], this work
SrLaGa ₃ O ₇ (SLG)	mellilite tetragonal uniaxial	8	0.56 1%	20648	28	126	70	56 [36]
Be ₂ La ₂ O ₅ (BLO)	monoclinic biaxial	10	2.35 1.2%	20496	4	186		68 this work
KPrP ₅ O ₁₄ (KPP)	tetraphosphate monoclinic biaxial	8	40 100%	20767	0.08	34	69	65 [37]

the optical frequency. Thus we have

$$\sigma_{\text{em}}(\nu) = \sigma_{\text{ab}}(\nu) \frac{g_l}{g_u} \exp\left(\frac{E_u - E_l}{kT}\right), \quad (2)$$

where $E_u - E_l$ is the energy gap between the manifolds.

The emission cross-section spectra together with the absorption cross-section spectra for each investigated material are presented in Fig. 2. The absorption band near 490 nm consists of transitions from the Stark levels of the ground state to the 3P_0 level when at shorter wavelengths the absorption to the 1I_6 , 3P_1 , and 3P_2 dominates. The cross-section values determined here are in reasonable agreement with reported literature data for Pr^{3+} doped YLF [11,31], YAP [30], and ZBLAN [34].

From Table I and Fig. 2 it is seen that in the investigated materials praseodymium exhibits a wide range of emission cross-sections from 2 to 12×10^{-20} cm² and fluorescence lifetime values from 0.08 to 40 μs . The main factors which determine the 3P_0 lifetimes are the radiative lifetimes, whose values calculated by means of the Judd-Ofelt theory are reported in the literature (see Table I), nonradiative

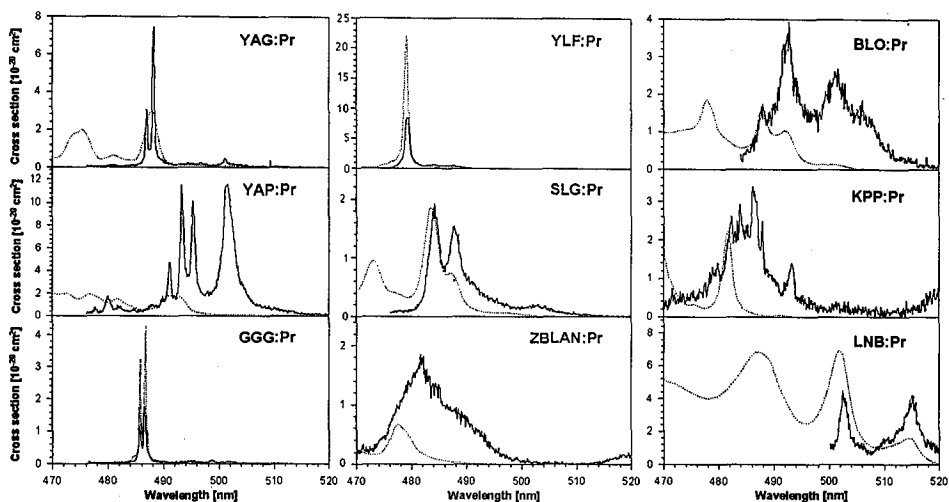


Fig. 2. Room temperature absorption and emission cross-section spectra of Pr^{3+} ion in various crystals.

decay rates and energy transfer (cross relaxation) rates, respectively. The longest lifetimes, of about $40 \mu\text{s}$, have been observed for low phonon fluoride compounds, i.e., YLF and ZBLAN glass, when oxides YAG, GGG, and YAP exhibit very similar lifetimes of about $10 \mu\text{s}$. The shortest lifetime of $0.08 \mu\text{s}$ observed in pentaphosphate is due to the very high energy of active phonons, up to 1300 cm^{-1} , and important cross relaxation resulting from the very high concentration of activator ions [37]. The reduced lifetime observed for LiNbO_3 is probably a manifestation of nonradiative decay via a fundamental absorption edge of the crystal which extends to the visible range and overlaps with the 3P_J manifolds. The 3P_0 level position, multiplet splittings, and the spacing of the energy levels reflect the nature of the crystal field which is determined in large part by the coordination polyhedron. Most of the investigated crystals exhibit a distorted eightfold site coordination, the twelfold and tenfold coordination of Pr^{3+} is found for YAP and BLO, respectively. Indeed, a weaker crystal field in these two materials results in a smaller splitting of energy levels and lower position of the 3P_0 level.

The emission and absorption cross-sections which are relevant to the operation of a blue praseodymium laser could also be determined by the oscillator strength calculated from the Judd–Ofelt theory. However, it is known that there are problems in describing the intensity of praseodymium transitions by this theory [33, 34] and that, due to the low lying $5d$ level which contributes to the oscillator strength of the $4f$ transitions, the Ω_i intensity parameter values (especially Ω_2) are poorly determined. Thus, also the theoretical treatment of the blue emission intensity, based on the fact that the corresponding branching ratio is controlled by the ratio of the Ω_2/Ω_4 parameters [39, 40], is not adequate. In the last column of Table I the theoretical and experimental values of branching ratios for the blue emission transition are compared.

3. Prediction of planar laser operation

In this section we analyse the threshold operation as well as dynamic behaviour of the transversely pumped waveguide laser structures with a Fabry–Perot and distributed feedback resonator, containing praseodymium as a lasing ion. Due to the scope of this paper the numerical results are only presented (without the loss of the generality) for distributed feedback lasers. It is worth noting that the distributed feedback lasers are very promising as a source of coherent light for fiber telecommunication and integrated optoelectronics, since they provide longitudinal mode selectivity and can be easily incorporated into optical circuits.

3.1. Threshold operation

In general, for many applications it is of essential importance to be able to design a laser for a given oscillation wavelength providing a maximal power efficiency. Unless additional selective elements are included in the laser cavity, the oscillation wavelength will, for a given loss, be determined by the spectral shape of the emission and absorption cross-sections. In general, because of the dependence of the spectral properties on host and index raising dopants, time consuming numerical analyses will normally be required to predict the laser operation [41].

In this section we present a fast and highly accurate method for prediction of the planar laser operation based on the measured spectral emission and absorption cross-sections. Our approach extends the method presented in Ref. [23] by taking into account the longitudinal field dependence of the laser mode and describes a laser structure with the distributed feedback.

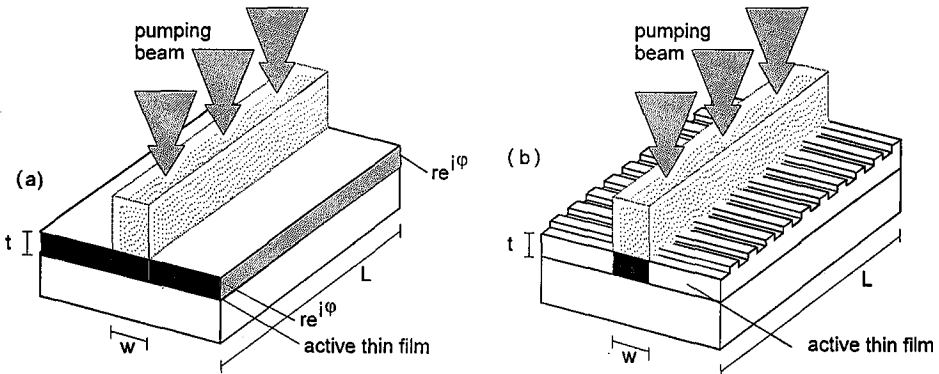


Fig. 3. Waveguide lasers considered in the paper: (a) laser structure with the Fabry–Perot resonator; (b) laser structure with distributed feedback.

In the case of the planar waveguide laser with the Fabry–Perot (F–P) resonator, see Fig. 3, the electric field of the counterpropagating waves $E_{mq}^{R,S}(x, t)$ of the mq -th laser mode can be written in the following form:

$$E_{mq}^R(x, z) = R_q(z)E_m(x) \quad \text{and} \quad E_{mq}^S(x, z) = S_q(z)E_m(x), \quad (3)$$

where the complex amplitudes, R_q and S_q , describe the longitudinal mode distribution. In our approach we assume that they can be approximated by the threshold

field distribution (see Ref. [42] for a detailed discussion). It is worth noting that this approximation has been verified for two-mirror lasers [42–45] as well as distributed feedback lasers [46–50]. Thus, in the case of the F–P resonator, according to [42], we have

$$|R_q(z)| = \exp(\gamma_q z) \quad \text{and} \quad |S_q(z)| = \frac{1}{R_2} \exp(-\gamma_q z), \quad (4)$$

where the propagation constant γ_q is equal to $\gamma_q = (1/2L) \ln[1/(R_1 R_2)]$ and $R_{1,2}$ denotes amplitude reflectivities at the end faces. $E_m(x)$ describes the transverse field distribution of the laser mode which is simultaneously the transverse field distribution of the m -th planar waveguide mode.

In this case the normalized to the laser length unsaturated net gain g (i.e., for the mode intensity the normalized small signal net gain) at the laser wavelength λ_1 can be expressed by

$$g = \Gamma L \rho [\langle i_0^e \rangle \sigma_e(\lambda_1) - (1 - \langle i_0^e \rangle) \sigma_a(\lambda_1)] (I_R + I_S) - 2A_q + \ln(R_1 R_2), \quad (5)$$

where L denotes the laser length, ρ denotes the ion density in the active medium, $\sigma_e(\lambda_1)$ and $\sigma_a(\lambda_1)$ are the emission and absorption cross-section, respectively, and $\langle i_0^e \rangle$ is the mean fraction of excited ions evaluated as

$$\langle i_0^e \rangle = \frac{1}{L} \int_0^L f(x = t/2, z) dz, \quad (6)$$

where $f(x, z)$ is the transverse fraction distributed function of excited ions and t is the thickness of the active waveguide. In Eq. (5) it is assumed that the effective number of excited ions interacting with the laser mode can be averaged into a product of the axial mean fraction $\langle i_0^e \rangle$, the modal confinement factor Γ , and the average longitudinal distribution intensities, I_R and I_S , of the counter-propagating waves of the laser mode

$$\int_0^t \int_0^L \rho i_e(x, z) I(x, z) dx dz \approx \Gamma (I_R + I_S) \rho L \langle i_0^e \rangle, \quad (7)$$

where the modal confinement factor Γ is defined as $\Gamma = \int_0^t |E_m(x)|^2 dx$ and the average longitudinal distribution intensities, I_R and I_S , are given in the threshold field approximation [42] by

$$I_R = \frac{1}{L} \int_0^L |R_q|^2 dz = \frac{1}{2\gamma_q L} \exp(2\gamma_q - 1) \quad (8)$$

and

$$I_S = \frac{1}{L} \int_0^L |S_q|^2 dz = \frac{1}{R_2^2} \frac{1}{2\gamma_q L} [1 - \exp(-2\gamma_q L)], \quad (9)$$

respectively. It is worth noting that in general I_R and I_S are different for the asymmetric structure. The average distributed loss in the structure is defined as

$$A_q = \int_0^L \alpha_1 (|R_q(z)|^2 + |S_q(z)|^2) dz, \quad (10)$$

where α_1 denotes the distributed loss coefficient in the structure.

In the case of the distributed feedback (DFB) planar laser (see Fig. 6) the electric field of the counter-propagating waves of the m -th laser mode in the threshold field approximation (see Refs. [46–51]) can be described by Eq. (3) with

$$R_q(z) = \sinh(\gamma_q z) \quad \text{and} \quad S_q(z) = \pm \sinh[\gamma_q(z - L)]. \quad (11)$$

The normalized small signal net gain in the structure can be expressed as

$$g = \Gamma L \rho [(i_0^e) \sigma_e(\lambda_l) - (1 - (i_0^e)) \sigma_a(\lambda_l)] (I_R + I_S) - 2A_q - 2g_{th}, \quad (12)$$

where the cavity losses resulting only from the coupling mechanism can be described by the net threshold gain g_{th} in the DFB structure with zero distributed losses which equals, according to Ref. [51],

$$g_{th} = \text{Re}\{\pm j\kappa \sinh(\gamma_q z)\} \quad (13)$$

and the propagation constant γ_q satisfies the eigenvalue equation

$$\gamma_q = \pm j\kappa \sinh(\gamma_q L), \quad (14)$$

where κ is the coupling coefficient and q is the number of DFB (longitudinal) mode. In this case the average longitudinal distribution intensities, I_R and I_S , are calculated by Eqs. (8) and (9) with R_q and S_q described by Eqs. (11), (13), and (14).

TABLE II

Comparison of the investigated Pr³⁺ activated planar waveguide parameters (λ_l — lasing wavelength, c.t.0 — critical thickness for TE₀, c.t.1 — critical thickness for TE₁, n_s — refractive index of the substrate, $n_f = n_s + 0.001$ — refractive index of the guided layers, n_c — refractive index of the cladding layer).

Waveguide structures	λ_l [μm]	c.t.0 [μm]	c.t.1 [μm]	n_s	Ref.	n_f	n_c
YAG:Pr	0.4882	1.1423	5.1635	$\sqrt{1 + \frac{2.2779\lambda^2}{\lambda^2 - 0.01142}} = 1.8419$	[52]	1.8429	1.0
GGG:Pr	0.48575	1.0857	4.9355	$\sqrt{1 + \frac{2.7382\lambda^2}{\lambda^2 - 0.01755}} = 1.9895$	[52]	1.9905	1.0
	0.48659	1.0876	4.9443	1.9893		1.9903	
YAP:Pr	0.4910	1.1089	5.0346	$\sqrt{1 + \frac{2.67792\lambda^2}{\lambda^2 - 0.012282}} = 1.9549$	[53]	1.9559	1.0
	0.4932	1.1140	5.0578	1.9546		1.9556	
	0.4953	1.1189	5.0796	1.9542		1.9552	
YLF:Pr	0.4794	1.2835	5.7019	$1.45909 + \frac{2756.3}{\lambda^2 [\text{nm}]} = 1.4711$	[32]	1.4721	1.0
ZBLAN:Pr	0.4816	1.2638	5.6980	$1.469 + \frac{3927}{\lambda^2 [\text{nm}]} = 1.48593$	[33]	1.48693	1.0
	0.4822	1.2654	5.7051	1.48598		1.48689	
LNB:Pr	0.5025	1.0110	4.6889	$2.207685 + \frac{0.032117}{\lambda^2} + \frac{0.000599}{\lambda^4} = 2.3443$	[54]	2.3453	1.0
	0.5151	1.0474	4.8140	2.3372		2.3382	
SLG:Pr	0.4878	1.1356	5.1365	$\sqrt{1 + \frac{2.2142\lambda^2}{\lambda^2 - 0.02297}} = 1.8576$	[55]	1.8586	1.0
BLO:Pr	0.4927	1.0717	4.8875	$\sqrt{1 + \frac{3.0725\lambda^2}{\lambda^2 - 0.01950}} = 2.0835$	[52]	2.0845	1.0
	0.5016	1.0918	4.9788	2.0810		2.0820	
KPP:Pr	0.4793	1.2101	5.4175	$\sqrt{1 + \frac{1.5740\lambda^2}{\lambda^2 - 0.00786}} = 1.6217$	[56,57]	1.6227	1.0
	0.4823	1.2178	5.4518	1.6214		1.6224	
	0.4833	1.2203	5.4632	1.6214		1.6224	
	0.4839	1.2219	5.4701	1.6213		1.6223	

The lasing will occur at a wavelength, where g in Eq. (5) (for a two-mirror laser) and Eq. (12) (for a distributed feedback laser) has a global maximum and, at the same time, fulfils the laser condition, i.e., $g = 0$. For the given laser length, mirror reflectivity (or in the case of the DFB laser coupling coefficient κ), thickness of the waveguide, distributed losses of the structure, and dopant concentration this determines both the laser wavelength λ_l and the mean fraction of the excited ions $\langle i_0^e \rangle$ required for the threshold operation.

We applied the presented approach to analyse the following planar waveguide lasers structures: (YAG:Pr³⁺)/YAG, (GGG:Pr³⁺)/GGG, (YAP:Pr³⁺)/YAP, (YLF:Pr³⁺)/YLF, (ZBLAN:Pr³⁺)/ZBLAN, (LNB:Pr³⁺)/LNB, (SLG:Pr³⁺)/SLG, (BLO:Pr³⁺)/BLO, (KPP:Pr³⁺)/KPP. We consider the strongest spectral lines in the blue range of the fluorescence spectrum, see Fig. 2. Our calculations have been carried out for a waveguide distributed feedback laser of a thickness $t = 2.5 \mu\text{m}$,

TABLE III

Summary of the spectroscopic properties of the investigated Pr³⁺ activated planar waveguides (λ_p — pumping wavelength, σ_p — absorption cross-section at the pumping, λ_l — lasing wavelength, σ_e — stimulated emission cross-section, σ_a — resonant absorption cross-section).

Waveguide structures	λ_p [μm]	σ_p [10^{-20} cm^2]	λ_l [μm]	σ_e [10^{-20} cm^2]	σ_a [10^{-20} cm^2]
YAG:Pr	0.452	6.35	0.4882	7.37	2.80
			0.4882	1.04	2.68
GGG:Pr	0.450	2.40	0.48659	1.38	2.48
			0.4910	4.76	1.79
YAP:Pr	0.449	2.20	0.4932	11.35	1.59
			0.4953	10.10	0.42
YLF:Pr	0.4792	21.94	0.4794	8.10	11.84
ZBLAN:Pr	0.465	0.68	0.4816	1.82	0.20
			0.4822	1.81	0.17
LNB:Pr	0.462	1.38	0.5025	4.49	6.56
			0.5151	4.23	1.50
SLG:Pr	0.4836	1.86	0.4878	1.54	0.69
BLO:Pr	0.453	1.77	0.4927	3.90	0.94
			0.5016	2.66	0.13
KPP:Pr	0.445	4.15	0.4793	1.50	0.40
			0.4823	2.61	1.55
			0.4833	2.49	0.51
			0.4839	2.91	0.33

which provides a fundamental transverse mode operation for all lasers considered, see Table II. It is worth noting that the propagation characteristics of the planar waveguides have been obtained including material dispersion of the medium. By putting the measured absorption and emission cross-section values, which are listed in Table III, into Eq. (12), for the given distributed loss coefficient α_1 and for the given coupling coefficient κ (which determines longitudinal field distribution as well as cavity losses, see Eqs. (11), (13), and (14)], the global maximum of g has been found for a certain wavelength λ_1 and a certain value of $\langle i_0^e \rangle$ for which simultaneously the laser condition $g = 0$ is fulfilled. The results obtained, showing the wavelength of the laser operation λ_1 as well the mean fraction of the excited ions $\langle i_0^e \rangle$ required to obtain laser operation, are presented in Table IV.

TABLE IV

Threshold parameters of the investigated waveguide distributed feedback lasers (λ_1 — lasing wavelength, λ_p — pumping wavelength, α_1 — distributed losses, κL — normalized optimal coupling coefficient, $\langle i_0^e \rangle$ — mean fraction of excited ions, ρ_{th} — threshold density of Pr^{3+} ions, P_{exc} — threshold pumping power).

Waveguide structure	λ_1 [μm]	λ_p [μm]	α_1	κL	$\langle i_0^e \rangle$	ρ_{th} [10^{19} cm^{-3}]	P_{exc} [10^3 W]
YAG:Pr	0.4882	0.452	0.01	30	0.616	6.525	0.356
GGG:Pr	0.48575		0.001	100	0.800	3.497	1.052
	0.48659	0.450	0.001	100	0.720	2.639	0.947
YAP:Pr	0.4910		0.01	100	0.713	5.017	1.227
	0.4932	0.449	0.01	30	0.555	4.084	0.955
	0.4953		0.01	30	0.574	4.628	0.987
YLF:Pr	0.4794	0.4792	0.01	30	0.810	7.398	0.040
ZBLAN:Pr	0.4816	0.465	0.001	100	0.534	2.694	0.839
	0.4822		0.001	100	0.531	2.721	0.835
LNB:Pr	0.5025	0.462	0.01	30	0.810	9.597	56.138
	0.5151		0.01	30	0.697	10.641	48.307
SLG:Pr	0.4878	0.4836	0.001	100	0.622	2.535	0.491
BLO:Pr	0.4927	0.453	0.01	30	0.613	11.215	3.801
	0.5016		0.01	30	0.737	16.995	4.570
KPP:Pr	0.4793				0.215	2.882	29.532
	0.4823	0.445	0.001	100	0.375	1.680	51.509
	0.4833				0.174	1.776	23.900
	0.4839				0.106	1.520	14.560

It is worth noting that the values of the coupling coefficient κ used in Eq. (12) provide a maximal power efficiency of the laser structure for a given loss level α_1 and for the normalized output power $P_{\text{out}}/P_s = 0.01$ (P_s is the saturation power). The optimal coupling coefficient values have been obtained (according to the energy theory, developed earlier for planar [49] and fiber [50] DFB lasers) by minimization of the following expression:

$$g(\kappa) = \frac{|\sinh(\gamma_q z)|^2 + \int_0^L \alpha_1 (|R_q(z)|^2 + |S_q(z)|^2) dz}{n_{(\text{eff})m} \int_{-\infty}^{\infty} |E_m(x)|^2 dx \int_0^t \int_0^L \frac{(|R_q(z)|^2 + |S_q(z)|^2) |E_m(x)|^2}{1 + (P_{\text{out}}/P_s)(|R_q(z)|^2 + |S_q(z)|^2) |E_m(x)|^2} dx dz}, \quad (15)$$

where R_q and S_q are described by Eqs. (11), (13), and (14), $E_m(x)$ describes transverse distribution of the m -th mode of the given waveguide structure and $n_{(\text{eff})m}$ is the effective index of the m -th waveguide mode. It is worth noting that in each iterative process of solving Eq. (12) the transverse field distribution has been recalculated for the each wavelength used (because of the material dispersion) in the trailing process.

In our paper we assume that the planar laser structures are excited by the transverse optical pumping, see Fig. 3. Thus, the threshold excitation power P_{exc} can be calculated from the following relation:

$$P_{\text{exc}} = \frac{Dt\lambda_{\text{exc}}tLw}{2\pi[1 - \exp(\alpha_{\text{ab}}t)\tau_{\text{fl}}]}, \quad (16)$$

where w is the width of the pumping area (in our case $w = 50 \mu\text{m}$), τ_{fl} is the fluorescence lifetime of the emitting level, λ_{exc} is the wavelength of the pumping beam and the absorption coefficient of the active medium α_{ab} is defined as

$$\alpha_{\text{ab}} = \sigma_{\text{ab}}(\lambda_{\text{exc}})\rho. \quad (17)$$

The excitation wavelength λ_{exc} as well as the pumping power P_{exc} and the minimal density of the Pr^{3+} ions required to obtain the threshold operation of the laser structures are also presented in Table IV.

As we can notice (see Table IV), the lowest excitation power required to obtain the threshold operation is available in (YLF: Pr^{3+})/YLF and (YAG: Pr^{3+})/YAG planar waveguide lasers. The relatively low threshold excitation is also obtained in (SLG: Pr^{3+})/SLG, (BLO: Pr^{3+})/BLO, and (ZBLAN: Pr^{3+})/ZBLAN laser structures. Moreover, for the given doping level and waveguide thickness the maximal available gain is again obtained in (YAG: Pr^{3+})/YAG and (YLF: Pr^{3+})/YLF planar laser structures.

In Table V we can observe a very interesting behaviour of the laser parameters. In this Table the wavelength of the laser operation λ_1 , the mean fraction of the excited ions (i_0^{e}) required to obtain the threshold operation, the threshold pumping power P_{exc} as well as the maximal gain available in the structure g_{max} are calculated for the (YAG: Pr^{3+})/YAG planar waveguide structure for various waveguide thicknesses. As we can notice, there exists an optimal waveguide thick-

TABLE V

Threshold parameters of the YAG:Pr waveguide structure for three various thickness of the active thin film.

Waveguide structure	Lasing wavelength λ_l [μm]	Pumping wavelength λ_p [μm]	Distributed losses α_1	Normalized coupling coefficient κL
YAG:Pr	0.4882	0.452	0.01	30
Waveguide structure	Thickness of active layer t [μm]	Mean fraction of excited ions $\langle i_0^e \rangle$	Threshold density of Pr^{3+} ions ρ_{th} [10^{19} cm^{-3}]	Threshold pumping power P_{exc} [W]
YAG:Pr	2.5	0.616	6.56	355.91
	10	0.320	0.84	185.50
	15	0.354	1.50	205.66

ness ($w = 10 \mu\text{m}$) for which the laser operation is obtained for the lowest pumping level. The optimal waveguide thickness depends on the lasing wavelength as well as on the doping level. Moreover, for this waveguide thickness we can simultaneously expect the maximal output power for a given pumping rate.

This effect can be explained as follows. On the one hand, there is an optimal waveguide thickness for which the length of the effective optical path for a given waveguide mode is the longest. This leads to the maximal effective gain available for the given waveguide mode — the waveguide effect. On the other hand, with the increasing waveguide thickness the rate of the absorbed power from the transverse pumping beam also increases resulting in the increasing number of the excited ions in the thin film. These two effects give an optimal waveguide thickness for which laser operation is obtained under the smallest pumping power and simultaneously for the given pumping rate for which the output power is maximal. It is worth noting that in general the optimal thickness of the planar waveguide is usually greater than the cut-off thickness of the higher order transfer modes. Thus, in this case the waveguide structure does not provide a single transverse mode operation.

In Tables VI and VII we present the maximal gain g_{max} available in the structure (obtained when the mean fraction of excited ions $\langle i_0^e \rangle$ is equal to unity) and the required pumping power P_{max} (in order to obtain g_{max}) as well as the differential pumping efficiency β defined as the ration of the increment of g to the increment of the pumping power P_{exc} , $\eta = \Delta g / \Delta P_{\text{exc}}$ [cm W^{-1}]. As we can notice, in the case of a single mode waveguide ($t = 2.5 \mu\text{m}$), the maximal pumping efficiency is obtained for (YLF:Pr³⁺)/YLF but the maximal gain is available in the (KPP:Pr³⁺)/KPP structure. Both discussed parameters are lasing wavelength dependent and, what is more, it is possible to maximize them by changing the waveguide thickness, as illustrated in Table VII.

TABLE VI

Maximal available gain and pumping efficiency of the investigated waveguide laser structures for the mean fraction of the excited ions $\langle \rho_0^* \rangle = 1$.

Waveguide structure	Lasing wavelength λ_l [μm]	Pumping wavelength λ_p [μm]	Pumping power P_{max} [10^4 W]	Maximal available gain g_{max} [10^{-2} cm^{-1}]	Pumping efficiency $\eta = \frac{\Delta g}{\Delta P_{\text{exc}}}$ [$\frac{10^{-5}}{\text{cm W}}$]
YAG:Pr	0.4882	0.452	0.058	8.780	34.787
GGG:Pr	0.48575	0.450	0.132	1.183	4.240
	0.48659			1.568	4.073
YAP:Pr	0.4910	0.449	0.172	3.481	8.470
	0.4932			8.407	10.422
	0.4953			7.300	9.571
YLF:Pr	0.4794	0.4792	0.005	6.871	612.194
ZBLAN:Pr	0.4816	0.465	0.157	0.723	0.894
	0.4822			0.716	0.879
LNB:Pr	0.5025	0.462	6.931	8.132	0.510
	0.5151			7.343	0.281
SLG:Pr	0.4878	0.4836	0.079	0.744	2.264
BLO:Pr	0.4927	0.453	0.620	8.667	1.366
	0.5016			5.720	0.856
KPP:Pr	0.4793	0.445	13.736	46.737	0.433
	0.4823			80.180	0.933
	0.4833			75.830	0.668
	0.4839			88.617	0.721

TABLE VII

Maximal available gain and pumping efficiency of the YAG:1%Pr waveguide laser structure for the mean fraction of excited ions $\langle \rho_0^* \rangle = 1$ and for three values of the active thin film thickness (λ_l — lasing wavelength, λ_p — pumping wavelength, t — thickness of an active layer, ρ_{th} — threshold density of Pr^{3+} ions, P_{max} — pumping power, g_{max} — maximal available gain, β — pumping efficiency).

Waveguide structure	λ_l [μm]	λ_p [μm]	t [μm]	ρ_{th} [10^{19} cm^{-3}]	P_{max} [W]	g_{max} [10^{-1} cm^{-1}]	β [$\frac{10^{-4}}{\text{cm W}}$]
YAG:Pr	0.4882	0.452	2.5	6.525	577.77	0.88	3.48
			10	0.8395	579.68	6.82	17.04
			15	1.497	580.85	3.83	9.92

3.2. Dynamic operation

In this section we analyse a dynamic operation of the planar waveguide lasers discussed above. In particular, we study relaxation oscillations and modulation bandwidth.

The relaxation oscillations can be a valuable tool in analysing various laser parameters, such as spontaneous lifetime and cavity losses. On the other hand, the modulation bandwidth is often used to describe the high-speed performance of high-data-rate lasers, which in general determines the rate of the optical data processing.

Starting from the rate equations and using a small vibration analysis it is possible to obtain for index coupling distributed feedback lasers the following expression for damping rate λ and frequency Ω of the relaxation oscillations [58, 59]:

$$\lambda = \frac{1}{t} \frac{\int_0^L \int_0^t [|R_q|^2 + |S_q|^2 + \eta(R_q^* S_q + S_q^* R_q)]^2 |E_{nm}(x)|^4 dx dz}{\int_0^L \int_0^t \frac{[|R_q|^2 + |S_q|^2 + \eta(R_q^* S_q + S_q^* R_q)]^2 |E_{nm}(x)|^4}{1+N[|R_q|^2 + |S_q|^2 + \eta(R_q^* S_q + S_q^* R_q)] |E_{nm}(x)|^2} dx dz} \quad (18)$$

and

$$\Omega^2 = \frac{N}{\tau_Q \tau} \frac{\int_0^L \int_0^t \frac{[|R_q|^2 + |S_q|^2 + \eta(R_q^* S_q + S_q^* R_q)]^2 |E_{nm}(x)|^4 dz dt}{1+N[|R_q|^2 + |S_q|^2 + \eta(R_q^* S_q + S_q^* R_q)] |E_{nm}|^2}}{\int_0^L \int_0^t \frac{[|R_q|^2 + |S_q|^2 + \eta(R_q^* S_q + S_q^* R_q)] |E_{nm}|^2 dz dt}{1+N[|R_q|^2 + |S_q|^2 + \eta(R_q^* S_q + S_q^* R_q)] |E_{nm}|^2}}, \quad (19)$$

where the modes amplitudes, R_q and S_q , are described for the Fabry–Perot laser by Eq. (4) and for the distributed feedback laser by Eq. (11), E_{nm} is the transverse field distribution of the appropriate waveguide mode, τ is the spontaneous lifetime, and the cavity lifetime τ_Q is defined as [58, 59]

$$\frac{1}{\tau_Q} = \frac{2c}{n_{(\text{eff})m} L} \times \left\{ |\sinh(\gamma_q L)|^2 + \int_0^L dz \alpha_1 [|R_q|^2 + |S_q|^2 + \eta(R_q^* S_q + R_q S_q^*)] \right\}, \quad (20)$$

where the speed of light is denoted by c and the normalization constant N is

$$N = \frac{P_{\text{out}}}{2 |\sinh(\gamma_q L)|^2 P_s}. \quad (21)$$

The damping rate λ and frequency of oscillations Ω in the planar waveguide laser with the Fabry–Perot resonator can be also described by Eqs. (17) and (18) with the mode amplitudes R_q and S_q given by Eq. (4). However, in this case the cavity lifetime τ_Q equals

$$\tau_Q = \left\{ \frac{c}{\eta_{(\text{eff})mn} L} \left[\frac{1}{R_2} \left(\frac{1 - R_1^2}{R_1} + \frac{1 - R_2^2}{R_2} \right) + 2 \int_0^L dz \alpha_1 (|R_q|^2 + |S_q|^2 + \eta(R_q S_q^* + R_q^* S_q)) \right] \right\}^{-1} \quad (22)$$

and the normalization constant N is given by

$$N = \frac{P_{\text{out}}}{\frac{1}{R_1} \left(\frac{1-R_1^2}{R_1} + \frac{1-R_2^2}{R_2} \right) P_s} \quad (23)$$

In Eqs. (18–20, 22), the parameter η distinguishes two cases: the first, $\eta = 0$, is addressed to the envelope field approximation (coherent terms are neglected) and the second one, $\eta = 1$, includes the spatial hole burning effect. It is worth noting that in general this parameter can take values from the region $(0, 1)$, describing the ability of the active medium to support the gain gradient.

In general, the frequency Ω and the damping rate λ of the relaxation oscillations determine also the 3-dB modulation bandwidth $f_{3\text{dB}}$, which often characterizes the high-speed performance of high-data-rate lasers. The modulation bandwidth $f_{3\text{dB}}$ is defined as the modulation frequency at which the small-signal response of the laser reduces itself by a factor of two relative to the zero frequency. It could be written in terms of the frequency Ω and the damping rate λ of the relaxation oscillations in the following way [60, 61]:

$$f_{3\text{dB}} = \frac{1}{2\pi} \sqrt{\Omega^2 - \lambda^2 + \sqrt{\Omega^2(\Omega^2 + \lambda^2) + \lambda^4}} \quad (24)$$

In Table VIII the parameters characterizing dynamic operation of the planar waveguide laser structures discussed are presented. As we can notice the maximal modulation bandwidth $f_{3\text{dB}}$ is obtained in the (KPP:Pr³⁺)/KPP structure. This is related to the fact that in this material the praseodymium fluorescence lifetime is the shortest, see also Table I. In Figs. 4–6, the damping rate λ , the frequency Ω

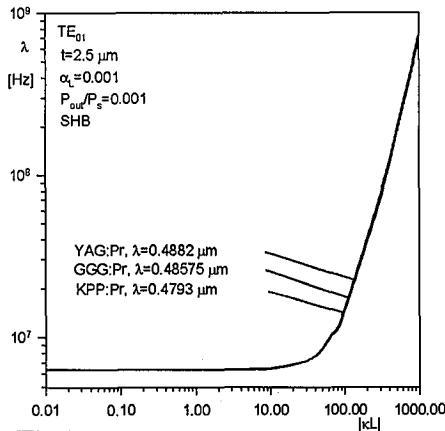


Fig. 4

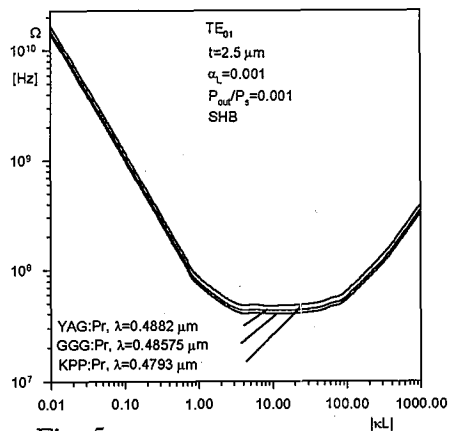


Fig. 5

Fig. 4. Damping rate λ of the relaxation oscillations as a function of the normalized coupling coefficient $|\kappa L|$ for various waveguide laser structures.

Fig. 5. Frequency Ω of the relaxation oscillations versus the normalized coupling coefficient $|\kappa L|$ for various waveguide laser structures.

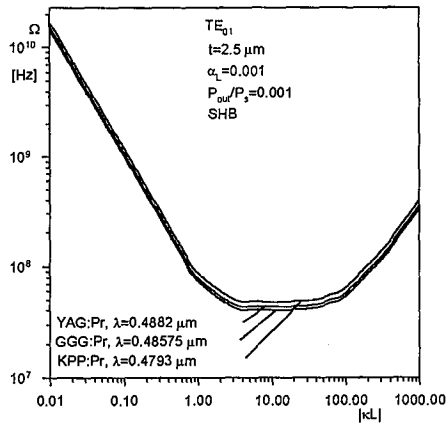


Fig. 6. Modulation bandwidth f_{3dB} as a function of the normalized coupling coefficient $|\kappa L|$ for various waveguide laser structures.

TABLE VIII

Dynamic parameters of the investigated Pr^{3+} activated planar waveguide distributed feedback lasers (index coupling coefficient $P_{out}/P_s = 1.0$, waveguide thickness $t = 2.5 \mu\text{m}$, fundamental mode TE_{01} including spatial hole burning effect SHB, λ_l — lasing wavelength, α_1 — normalized losses, K_L — optimal coupling coefficient, $g_0 L$ — small signal gain, λ_r — dumping rate, Ω — relaxation oscillation frequency, f_{3dB} — modulation bandwidth).

Waveguide structures	λ_l [μm]	α_1	K_L	$g_0 L$	λ_r [10^8 s^{-1}]	Ω [10^8 s^{-1}]	f_{3dB} [10^8 Hz]
YAG:Pr	0.4882	0.01	30	30.733	0.109	1.606	0.443
GGG:Pr	0.48575	0.001	100	13.256	3.771	2.388	0.827
	0.48659	0.001	100	13.280	3.763	2.391	0.827
YAP:Pr	0.4910	0.001	100	13.540	4.419	2.668	0.947
	0.4932	0.01	30	30.057	0.123	1.619	0.446
YLF:Pr	0.4953	0.01	30	30.208	0.122	1.624	0.448
	0.4794	0.01	30	35.703	0.034	1.187	0.327
ZBLAN:Pr	0.4816	0.001	100	16.260	1.156	1.901	0.531
	0.4822	0.001	100	16.307	1.155	1.906	0.533
LNB:Pr	0.5025	0.01	30	28.806	3.340	7.572	2.096
	0.5151	0.01	30	29.522	3.251	7.679	2.125
SLG:Pr	0.4878	0.001	100	13.844	1.811	1.794	0.533
BLO:Pr	0.4927	0.01	30	29.050	0.372	2.626	0.724
	0.5016	0.01	30	29.603	0.365	2.657	0.733
KPP:Pr	0.4793	0.001	100	14.845	604.01	37.777	96.507
	0.4823	0.001	100	15.003	600.28	38.094	95.921
	0.4833	0.001	100	15.057	599.05	38.204	95.729
	0.4839	0.001	100	15.091	598.32	38.271	95.615

of the relaxation oscillations, and the 3-dB modulation bandwidth f_{3dB} are also shown as a function of the coupling strength $|\kappa L|$ with the spatial hole burning effect included, $\eta = 1$. It is worth noting that the frequency Ω of the relaxation

oscillations as well as the 3-dB modulation bandwidth f_{3dB} characteristics exhibit minima for these values of the coupling coefficient for which a maximal power efficiency of the laser structure is obtained (for a detailed discussion see Refs. [60, 61]).

4. Conclusions

The spectroscopic properties relevant to blue laser action have been determined for various Pr^{3+} activated materials. It is shown that on the basis of the simple spectroscopic measurements it is possible to develop a more complete picture of the potential performance of blue wavelength waveguide structures.

The key results of the presented model are expressions for the threshold and gain dependences on pump power and for dynamic parameters of the planar waveguide blue laser with the Fabry–Perot as well as distributed feedback resonators. These equations include constants, such as the cross-sections and lifetimes, easily obtained by simple spectroscopic measurements. The absorption and emission cross-section spectra for transitions between the ground 3H_4 and the upper 3P_0 levels of Pr^{3+} ion have been determined for nine hosts.

From our analysis it results that the efficiency of the transverse pumped planar laser will require large absorption cross-sections at a pumping wavelength and has its optimum for a certain waveguide thickness, which generally is larger than the one required for fundamental mode operation.

Among the various hosts we have studied, the lowest threshold was predicted for Pr^{3+} :YAG/YAG waveguides. However, the calculated threshold pump power P_{th} value of about 200 W demonstrates a practical difficulty in the transverse pumping of the waveguide lasers. It is anticipated that longitudinal pumping presents advantages in terms of lower laser excitation threshold, and will be considered in a forthcoming paper.

Moreover, the compromise between the possible maximal available value of the modulation bandwidth and maximal available power efficiency in these waveguide structures is required. However, in general, the modulation bandwidth available in these lasers is smaller than in high-data-rate semiconductor lasers, where the high nonlinear dispersion effect (caused by the strong electro–optical coupling) enhances the modulation process. Thus, in the case of planar waveguide dielectric laser structures if we require the modulation bandwidth to be greater than 1 GHz it is preferential to use an external modulator, for example the integrated electrooptic waveguide one.

References

- [1] E.A. Downing, L. Heselink, R.M. Macfarlane, C.P.J. Barty, in: *Conf. Lasers and Electro-Optics CLEO'94, Anahaim (Ca)*, Vol. 8, Technical Digest Series, Optical Society of America, Washington (DC) 1994, paper CMB1.
- [2] S.G. Anderson, *Laser Focus World* **29**, 27 (1993).
- [3] T.V. Higgins, *Laser Focus World* **29**, 57 (1993).
- [4] L.R. Marshall, *Laser Focus World* **29**, 185 (1993).
- [5] M. Haase, J. Qiu, J. DePuydt, H. Cheng, *Appl. Phys Lett.* **59**, 1272 (1991).
- [6] T.S. Fan, R.L. Byer, *IEEE J. Quantum Electron.* **24**, 895 (1988).

- [7] A. Ashkin, G.D. Boyd, J.M. Dziedzic, *IEEE J. Quantum Electron* **QE-2**, 109 (1996).
- [8] A.J. Silversmith, W. Lenth, R.M. Macfarlane, *J. Opt. Soc. Am. A* **3**, 128 (1986).
- [9] J.Y. Allain, M. Monerie, H. Poignant, *Electron. Lett.* **26**, 166 (1990).
- [10] L. Esterowitz, R. Allen, M. Krueer, F. Bartoli, L.S. Goldberg, H.P. Jenssen, A. Linz, V.O. Nicolai, *J. Appl. Phys.* **48**, 650 (1977).
- [11] T. Sandrock, T. Danger, E. Heumann, G. Huber, B.H.T. Chai, *Appl. Phys. B* **58**, 149 (1994).
- [12] T. Danger, T. Sandrock, E. Heumann, G. Huber, B. Chai, *Appl. Phys. B* **57**, 2399 (1993).
- [13] M. Malinowski, M.F. Joubert, B. Jacquier, *Physica Status Solidi A* **140**, K49 (1993).
- [14] M. Malinowski, M.F. Joubert, R. Mahiou, B. Jacquier, *J. Phys. IV C* **4**, 541 (1994).
- [15] J.Y. Allain, M. Monerie, H. Poignant, *Electron. Lett.* **27**, 1156 (1991).
- [16] J.Y. Allain, M. Monerie, H. Poignant, *Electron. Lett.* **27**, 189 (1991).
- [17] D. Piehler, D. Craven, N. Kwong, H. Zarem, *Electron. Lett.* **29**, 1857 (1993).
- [18] Y. Zhao, S. Fleming, S. Poole, *Optics Commun.* **114**, 285 (1995).
- [19] J.G. Grabmaier, B.C. Grabmaier, R.Th. Kersten, R.D. Plattner, G.J. Zeidler, *Phys. Lett. A* **43**, 219 (1973).
- [20] D. Pelenc, B. Chambaz, I. Chartier, B. Ferrand, C. Wyon, D.P. Shepherd, D.C. Hanna, A.C. Large, A.C. Tropper, *Optics Commun.* **115**, 491 (1995).
- [21] L. Zhang, P.D. Townsend, P.J. Chandler, A.J. Silversmith, *Electron. Lett.* **30**, 1063 (1994).
- [22] E. Snoeks, Ph.D. Thesis, Utrecht University, Utrecht 1995.
- [23] A.O. Nielsen, J.H. Povlesen, A. Bjarklev, O. Lumholt, T.P. Rasmussen, K. Rottwit, *Electron. Lett.* **17**, 1664 (1991).
- [24] P. Szczepański, A. Mossakowska-Wyszyńska, M. Malinowski, Z. Łuczyński, T. Łukasiewicz, Z. Frukacz, in: *Conf. on Lasers and Electro-Optics Europe, CLEO'94, Amsterdam*, IEEE Cat. Nr.94TH0614-8, paper CTuK48, 1994, p. 120.
- [25] P. Szczepański, A. Tyszka-Zawadzka, M. Malinowski, Z. Łuczyński, T. Łukasiewicz, Z. Frukacz, in: *Conf. on Lasers and Electro-Optics Europe, CLEO'94, Amsterdam*, IEEE Cat.Nr. 94TH0614-8, paper CTuK73, 1994, p. 134.
- [26] B.R. Judd, *Phys. Rev.* **127**, 750 (1962).
- [27] G.S. Ofelt, *J. Chem. Phys.* **37**, 511 (1962).
- [28] M. Malinowski, R. Wolski, W. Woliński, *Solid State Commun.* **74**, 17 (1990).
- [29] N. Raspa, Ph.D. Thesis, Concordia University, Montreal (Canada) 1992.
- [30] T. Danger, A. Bleckmann, G. Huber, *Appl. Phys. B* **58**, 413 (1994).
- [31] D.S. Knowles, Z. Zhang, D. Grabbe, H.P. Jenssen, *IEEE J. Quantum Electron.* **24**, 1118 (1988).
- [32] J.L. Adam, W.A. Sibley, D.R. Gabbe, *J. Lumin.* **33**, 391 (1985).
- [33] R.S. Quimby, W.J. Miniscalco, *J. Appl. Phys.* **75**, 613 (1994).
- [34] A.C. Tropper, J.N. Carter, R.D.T. Lauder, D.C. Hanna, S.T. Davey, D. Szebesta, *J. Opt. Soc. Am. B* **11**, 886 (1994).

- [35] A. Lorenzo, L.E. Bausa, J. Garcia Sole, *Phys. Rev. B* **51**, 16643 (1995).
- [36] M. Malinowski, I. Pracka, B. Surma, T. Łukasiewicz, W. Woliński, R. Wolski, *Optical Materials* **6**, 305 (1996).
- [37] M. Malinowski, R. Wolski, W. Woliński, *J. Lumin.* **35**, 1 (1986).
- [38] D.E. McCumber, *Phys. Rev. A* **136**, 954 (1964).
- [39] R. Reisfeld, C.K. Jorgensen, *Excited State of Rare Earth*, Springer-Verlag, Berlin 1977.
- [40] K. Hirao, M. Higuda, N. Soga, in: *Int. Conf. on Luminescence ICL,93, Univ. of Connecticut, Storrs, CT USA*, Technical Digest, Tu5-11, 1993.
- [41] B. Henderson, G.F. Imbusch, *Optical Spectroscopy of Inorganic Solids*, Calendon Press, Oxford 1989.
- [42] A. Kujawski, P. Szczepański, *J. Mod. Opt.* **38**, 1901 (1991).
- [43] K. Janulewicz, P. Szczepański, *Appl. Opt.* **30**, 3818 (1991).
- [44] A. Kujawski, P. Szczepanski, *J. Mod. Opt.* **39**, 2519 (1992).
- [45] P. Szczepański, P. Witoński, *Appl. Opt.* **34**, 6099 (1995).
- [46] P. Szczepański *Appl. Opt.* **24**, 3574 (1985).
- [47] P. Szczepański, *IEEE J. Quantum Electron.* **22**, 517 (1986).
- [48] P. Szczepański, *J. Appl. Phys.* **63**, 4854 (1988).
- [49] P. Szczepański, D. Sikorski, W. Woliński, *IEEE J. Quantum Electron.* **25**, 871 (1989).
- [50] P. Szczepański, M. Sklodowska, W. Woliński, *J. Lightwave Technol.* **9**, 329 (1991).
- [51] H. Kogelnik, C.V. Shank, *J. Appl. Phys.* **43**, 2327 (1972).
- [52] T.S. Lomhaim, L.G. De Shazer, *Phys. Rev. B* **20**, 4343 (1979).
- [53] Y. Kuwano, *J. Appl. Phys.* **49**, 4223 (1978).
- [54] C.A. Morrison, R.P. Leavit, in: *Handbook on the Physics and Chemistry of Rare Earth*, Eds. K.A. Gschneidner, L. Eyring, North-Holland Publ. Co., 1982, p. 461.
- [55] F. Hanson, D. Dick, H.R. Verdun, M. Kokta, *J. Opt. Soc. Am B* **8**, 1668 (1991).
- [56] J. Nakano, *J. Appl. Phys.* **52**, 1239 (1981).
- [57] B.N. Litvin, G.U. Dorohova, O.S. Filipienko, *Dokl. A.N. USSR* **259**, 1102 (1981).
- [58] P. Szczepański, A. Mossakowska, D. Dejnarrowicz, *J. Lightwave Technol.* **10**, 220 (1992).
- [59] A. Mossakowska, P. Szczepański, W. Woliński, *Opt. Commun.* **100**, 153 (1993).
- [60] A. Mossakowska, P. Szczepański, W. Woliński, *IEEE J. Quantum Electron.* **30**, 230 (1994).
- [61] A. Mossakowska-Wyszyńska, P. Szczepański, *Opt. Commun.* **118**, 61 (1995).